Geomorphology 123 (2010) 142–153

Contents lists available at ScienceDirect

Geomorphology

journal homepage: www.elsevier.com/locate/geomorph

Geomorphic assessment of the debris avalanche deposit from the Jocotitlán volcano, Central Mexico

Sergio Salinas *[,1], Jorge López-Blanco

Depto. de Geografía Física, Instituto de Geografía, Universidad Nacional Autónoma de México, Ciudad Universitaria, C. P. 04510, México, D.F., México

ARTICLE INFO

Article history:
Received 25 July 2009
Received in revised form 8 July 2010
Accepted 9 July 2010
Available online 15 July 2010

Keywords:
Jocotitlán volcano
Geomorphometry
Principal components
Cluster analysis
Hummocks
Ridges

ABSTRACT

Edifice collapse of the Jocotitlán volcano produced a debris avalanche deposit whose morphology is characterized by conical hummocks and elongated ridges. We consulted aerial photographs, orthophotographs, and conducted field work to define field relationships between mound morphology and stratigraphy. Based on field evidence and geomorphic and geologic interpretation we sub-divide the deposit into three sectors (north, northeastern, and eastern). We determine the emplacement mechanisms of the different sectors based on their distinct morphologic and lithologic features. In this context, we generate a geomorphometric database comprising 17 variables for each mound and apply multivariate statistical methods (principal component analysis and cluster analysis) to define the relationships between them. The principal components incorporated 73% of the total data variance and seven geomorphometric variables (perimeter, major axis, area, height, distance to the source, axis ratio and circularity index) defined two groups: hummocks and ridges. The circularity index and the axis ratio best characterize the elongated form of hummocks composing the deposits. Contrasts in lithological characteristics, such as material strength and mobility, provide evidence for a transition from a sliding mass (debris avalanche deposit) to a debris-flow-like emplacement. Differences in deposit morphology suggest two collapse mechanisms: magmatic intrusion (Bezymianny-type sector collapse) and a tectonic mass-slide, an earthquake could provide the trigger for both collapses. The eastern lower flank of the volcano then collapsed gravitationally due to a movement along a fault (tectonic activity possibly related to the Acambay–Tixmadeje Fault System). This produced the northeastern sector of the debris avalanche deposit dominated by large elongated ridges. The spatial arrangement of both sectors (the N and NE) suggests that the two failure events occurred simultaneously. Finally, the eastern sector of the deposit was emplaced by posterior remobilization of material from the two other sectors through a debris flow.

1. Introduction

1.1. Volcanic debris avalanche deposits

Major edifice collapse is a common phenomenon in the growth history of many composite volcanoes. It occurs mainly in andesitic to rhyolitic stratovolcanoes (e.g. Mt. St. Helens in 1980 — Lipman and Mullineaux, 1981; Siebert, 1984; Siebe and Sheridan, 1990). The instability and weakening of a volcanic edifice is the result of several factors, which include repeated magmatic intrusions and emplacement of the volcano in a tectonically active region prone to large earthquakes (Francis and Wells, 1988; Voight and Elsworth, 1997). Seismic activity not only directly affects the stability of the volcanic edifice but may also deform its basement, weakening the volcanic edifice (Borgia et al., 2000).

A debris avalanche is a rapidly moving, incoherent, water-undersaturated mass made-up of a mixture of blocks, sand, and silt which flows under the influence of gravity. There are three principal processes which can trigger the collapse of a volcano: 1) a volcanic eruption (magmatic intrusion), 2) a phreatic explosion or alteration (i.e. hydrothermal alteration), and 3) seismic–tectonic activity (Siebert et al., 1987). The direction of edifice failure depends on structural lineaments, which usually correspond with the direction of maximum distension in the tectonic regime (Voight and Elsworth, 1997).

The resulting topography of the collapse sector is a debris avalanche deposit (DAD) that is morphologically characterized by mounds. For this study we distinguish two types of mounds: 1) hummocks or mounds with irregular-to-conical form with no elongation, and 2) elongated mounds or ridges which, depending on the main direction of the flow, can be transverse or longitudinal to the flow direction (Siebert, 1984). Both types of mounds compose a hilly topography proximal to the volcano and decrease in size and number towards more distal parts. Generally, the deposit is bordered by prominent marginal levees and characterized by small closed basins forming between hummocks

* Corresponding author. +52 5 6224119x20; fax: +52 5502486.
E-mail address: sss@geofisica.unam.mx (S. Salinas).
[1] Present address: Depto. de Volcanología, Instituto de Geofísica, Universidad Nacional Autónoma de México, Ciudad Universitaria, C.P. 04510, México, D.F., México.

0169-555X/$ – see front matter © 2010 Elsevier B.V. All rights reserved.
doi:10.1016/j.geomorph.2010.07.006

(Glicken, 1991). Dufresne and Davies (2009) note that longitudinal ridges are often oriented parallel to flow directions, and disposed radially with respect to the source at proximal distance due to the lateral spreading of the mass flow. Therefore the flow direction of the debris avalanche is indicated by the trajectory of the long or longitudinal axis of the mounds (Dufresne and Davies, 2009). In distal parts, transverse ridges can be produced by compression or deceleration of the sliding mass when it impacts a topographic barrier or when the avalanche enters the sea (e.g. Augustine volcano — Siebert et al., 1995).

The spatial distribution and geomorphology of the mounds depend mostly on the material composing them, the trigger mechanism of the collapse, the runout distance, and the age of the deposit (degree of erosion and land cover). The lithologic facies describe the internal structure of the DAD which is determined by the changes that the material experiences during transportation (Palmer et al., 1991). Flow dynamics can alter the competence of the material with respect to its original characteristics. Debris avalanche lithofacies are classified into three types: 1) block lithofacies, composed mainly of blocks (>1 m in size) with a minor volume (<30 vol.%) of sandy interclast matrix (all components of the deposit comprising material <2 mm in diameter); 2) mixed lithofacies, composed mainly of clasts (2 mm to 1 m in size), a moderate proportion in the volume of sandy interclast matrix (between 30 and 90 vol.%) and few blocks; and 3) marginal lithofacies, composed of few clasts (ca. 10 vol.%) amongst sandy interclast matrix (Palmer et al., 1991). Longer runout distances allow the disaggregation of the material, reducing the size, height, and flank steepness of the hummock or ridge.

Sector collapse of the Jocotitlán volcano produced a major DAD characterized by a hummocky topography (Fig. 1) and elongated ridges with distinct geometry. The primary objectives of this study were to compare the morphologic characteristics, distribution, and arrangement of the DAD and apply quantitative criteria to understand its emplacement mode and origin. The morphological differences between specific parts of DAD are keys to understanding the processes that generated them (Siebe and Sheridan, 1990; Siebert, 1996). Therefore, by evaluating the patterns in the spatial distribution of specific features and differences in the nature of the material composing the Jocotitlán DAD, the degree of fracturing and the emplacement mode can be determined and the processes associated with the collapse are thus inferred.

1.2. Approach

Following the division of geomorphometry proposed by Evans (1972) into general and specific geomorphometry, this study focuses on the measurement and analysis of landforms that are from adjacent parts of the surface, by applying a clear-cut constraint criterion. The variables are closely related to the processes of formation, which makes the use of specific geomorphometry more useful than general geomorphometry as we are dealing with topographic landforms that have a single origin (Evans, 1987). Setting up constraints on the studied landforms is particularly relevant to this type of study. A number of metric variables are extracted from each of the defined geomorphic groups. This yields a complex database, which makes it necessary to apply a multivariate statistical analysis to solve the genetic and factor relations between these different variables (Pike, 1974). Doing so, we can reduce the database (number of variables) without losing important information (Castillo-Rodríguez et al., 2007) and also identify the variables that are highly correlated, and thus most relevant for the interpretation.

2. Regional geologic framework

2.1. Tectonic setting

The Jocotitlán volcano (3952 m.a.s.l.) is located in the central part of the Mexican Volcanic Belt (MVB) (Fig. 2A). The MVB is a volcanic arc which cuts across the Mexican Republic between 19° and 20° N and consists of a wide variety of volcanic rocks that include extensive lava plateaus (mesas), scoria cone fields, domes, stratovolcanoes, and ignimbrites produced by caldera formation (Macías, 2007 and references therein). Numerous volcanoes in the MVB, such as Volcán de Colima, Nevado de Colima, Nevado de Toluca, Iztaccíhuatl, Popocatépetl, Pico de Orizaba, and Las Derrumbadas, have undergone major collapses during their eruptive history (Siebe et al., 1995; Capra et al., 2002).

Although several models have been proposed to explain the origin of the MVB, most authors relate it to the northeast-trending subduction of the Cocos and Rivera plates underneath the North American plate along the Mesoamerican Trench (Fig. 2A) (Ferrari et al., 1994, Macías, 2007). Based on seismic tomography data, dynamic reconstruction and geological records, Ferrari (2004) proposed a slab detachment underneath the MVB during the late Miocene.

Field observations, petrologic and isotopic data, and geochronological age constraints indicate that the magmatic activity in the MVB has migrated, which complicates sector division (Suter et al., 1992; Ferrari et al., 1994; Schaaf et al., 2005). Based on structural evolution, Ferrari et al. (1994) divided the MVB into three sectors: western, central and eastern. The Jocotitlán volcano is located in the central sector.

The Jocotitlán volcano is located between two important fault systems: the Taxco–Querétaro (TQFS) and the Acambay–Morelia (AMFS) (Fig. 2B). The TQFS is a 20 to 40 km wide and 250 km long regional system, which extends from Taxco in the south to Querétaro in the north. There are several volcanoes aligned along this fault system: the Amealco caldera, and the La Joya, San Antonio, and the Nevado de Toluca volcanoes (García-Palomo et al., 2000). The Perales normal fault belongs to the TQFS and is the closest fault to the Jocotitlán volcano,

Fig. 1. Photograph of the Jocotitlán volcano viewed from the N. Notice the conical morphology of the proximal hummocks and the adjacent dome to the NW of the main edifice.

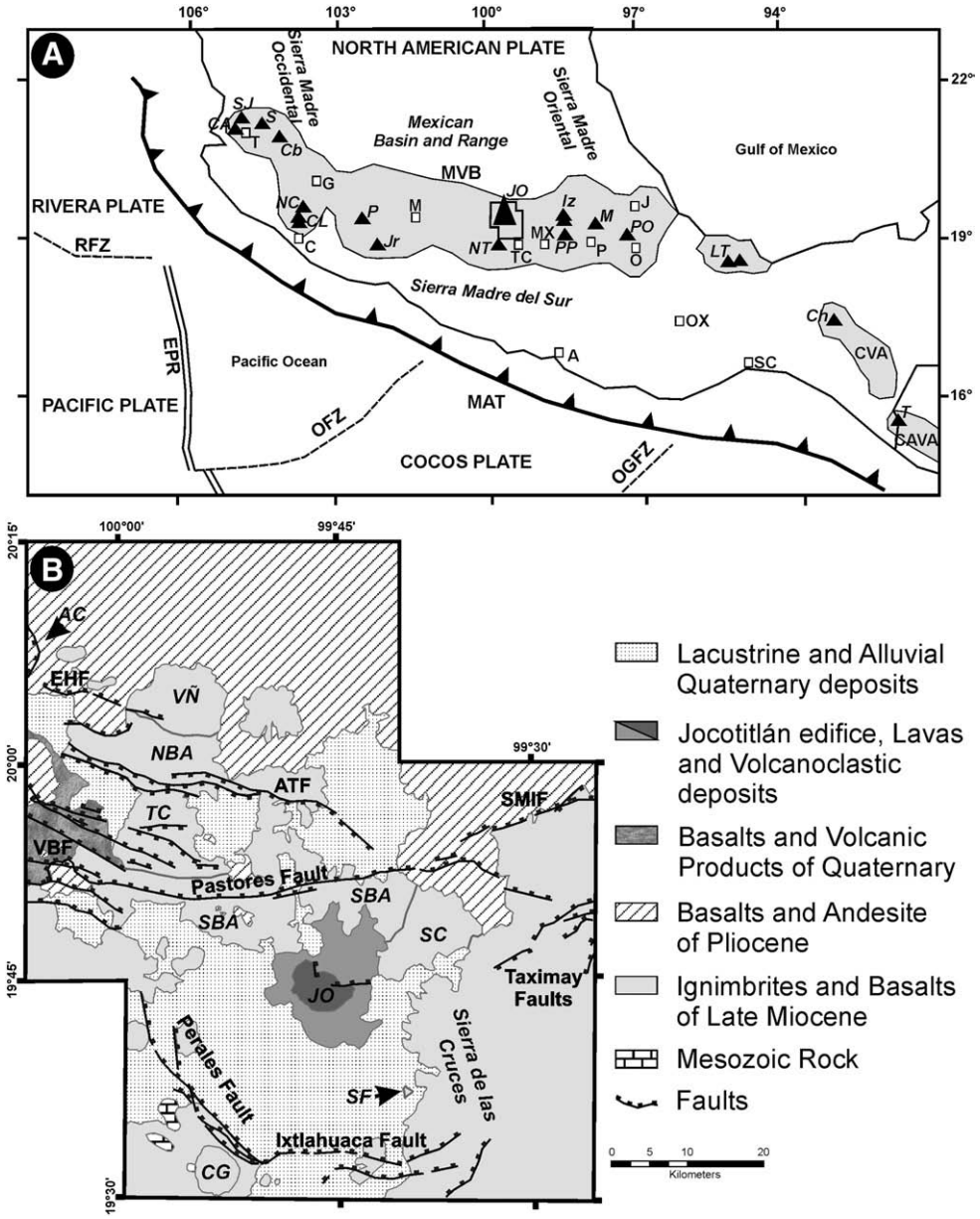

Fig. 2. Maps showing the major volcanic structures in the vicinity of the Jocotitlán volcano. A) Shows the regional tectonic and geodynamic setting of the Mexican Volcanic Belt, the main volcanoes (italic letters and filled triangles), and cities (white squares). Abbreviations: MAT, Middle American Trench; EPR, East Pacific Rise; RFZ, Rivera Fracture Zone; OFZ, Orozco Fracture Zone; OGFZ, O'Gorman Fracture Zone; CVA, Chiapanecan Volcanic Arc and CAVA, Central American Volcanic Arc. Cities: T, Tepic; G, Guadalajara; C, Colima; M, Morelia; TC, Toluca; MX, México; P, Puebla; O, Orizaba; J, Jalapa; A, Acapulco, OX, Oaxaca; SC, Salina Cruz; Volcanoes: SJ, San Juan; CG, Cerro Alto; S, Sanganguey; Cb, Ceboruco; NC, Nevado de Colima; CL, Volcán de Colima; Jr, Jorullo; P, Parícutin; NT, Nevado de Toluca; JO, Jocotitlán; Iz, Iztaccíhuatl; PP, Popocatéptl; M, La Malinche; PO, Pico de Orizaba; LT, Los Tuxtlas; Ch, Chichón and T, Tacaná. B) Tectonic and geologic settings of the Jocotitlán volcano. Map of the Jocotitlán volcano shows the main faults of the region (modified from Martínez-Reyes and Nieto-Samaniego, 1990). Abbreviations: CG, Cerro La Guadalupana; SF, Twin domes of San Felipe del Progreso; SC, Sierra de Coamango (Range); JO, Jocotitlán volcano; TC, Temascalcingo caldera; VÑ, Ñado Volcano; AC, Amealco caldera; NBA, North Block of Acambay graben; SBA, South Block of Acambay graben; VBF, Venta de Bravo fault; EHF, Epitacio Huerta fault; SMIF, Santa María Ilucan fault and ATF, Acambay–Tixmadeje fault.

located just to the SW of the edifice. It strikes NNW–SSE and extends ~50 km from the northern part of Cerro La Guadalupana to the western slopes of Sierra de las Cruces, where it merges with the E–W trending Ixtlahuaca fault (Fig. 2B) (García-Palomo et al., 2008).

The AMFS is composed of large normal faults that bound a topographically well-defined graben, known in the vicinity of the Jocotitlán volcano as the Acambay graben. On a regional scale, the AMFS trends E–W and cuts several large volcanic structures and a few scoria cones. Such faults are widely distributed and are currently active (Suter et al., 1992). The Pastores fault is the most visible structural feature to the north of the Jocotitlán volcano. This normal fault represents the southern wall of the Acambay graben and extends for 25 km. The Acambay–Tixmadeje fault (ATF), is part of the northern wall of the Acambay graben, and is located opposite to the Pastores fault. The ATF is represented by normal faults oriented ESE–WNW that extend for 40 km (Fig. 2B). The Perales, Ixtlahuaca, and Pastores faults are part of a tectonic graben known as the Ixtlahuaca graben (Ortiz and Bocco, 1989) near the center of which the Jocotitlán volcano is located (Fig. 2B).

2.2. Geology of Jocotitlán volcano

The volcanic edifice is made of interlayered andesitic and dacitic lavas with intercalated pyroclastic deposits. Siebe et al. (1992) assign

an age of 680 ± 90 ^{14}C years B.P. to a pyroclastic surge deposit and a block-and-ash-flow deposit on the upper flanks of the edifice. These deposits are the result of the most recent eruptive event. A complex of dacitic–andesitic lava flows are distributed W–NW of the main summit and form a dome-like structure (Fig. 1), which gives the entire volcano an asymmetric E–W elongation. A horseshoe-shaped crater and a major scarp which faces to the N are the most remarkable features of the volcano. The upper flanks, consisting of massive to strongly flow-banded dacitic lava flows, are steep and display a convex-upward shape. In contrast the lower flanks are gently concave-upward slopes composed of a series of andesitic lava flows (Fig. 1).

The collapse was associated with a major volcanic activity dated at 9690 ± 85 ^{14}C years B.P. (Siebe et al., 1992). The DAD can be identified by large conical hummocks and large elongated ridges with an E–W direction. Overlying the DAD, Siebe et al. (1992) described a 3 m of a pyroclastic fallout sequence, which they interpreted as being derived from a magma that was present within the edifice when it fractured and failed.

The DAD is clast-supported and poorly sorted. It consists of a mixture of angular to sub-angular clasts of porphyritic andesitic to dacitic lava (60–67% SiO_2) with phenocrysts of clinopyroxene, orthopyroxene and abundant plagioclase (Siebe et al., 1992). The deposit is extremely heterometric with the majority of the volume composed of clasts and blocks ranging from 1 to 5 m in size, whereas fine material (sand-sized) is minor in proportion. The fine material is considered to be the product of the shattering of the blocks during sliding and flow of the mass (Siebe et al., 1992). Cores of the conical hummocks are typically mega-blocks (10–20 m in length) surrounded by smaller fragments piled up at the angle of repose (Siebe et al., 1992). Pyroclastic deposits which overlie the avalanche deposit outcrop in the eastern sector. The lowermost part of the pyroclastic deposit consists of a tephra sequence interlayered between laminated and massive beds (1.5–2 m in thickness). The deposit is composed of coarse ash, sub-angular pumice lapilli (2–4 cm in diameter), dark lithic fragments of dense porphyritic lava, and angular obsidian clasts (0.5–1 cm in diameter).

3. Methodology

The DAD shows an exceptional morphology with a very peculiar geometrical shape. It is made of two geometrically distinct types of mounds: conical hummocks and elongated ridges. The entire deposit can be morphologically divided into three sectors: north, northeastern and eastern sectors (Fig. 3). We determined the geomorphometric variables (Table 1) to identify the meaningful variations in the deposit. The mounds of the deposit were outlined and verified in the field (Fig. 3) using 1:37 500 scale panchromatic aerial photographs from IGECEM (Instituto de Investigación Geográfica, Estadística y Catastral del Estado de México; the official geographical and mapping institute of the State of Mexico), and a digital terrain model (DTM), which was created in the ILWIS GIS by rasterizing the 10 m contour levels from the 1:50 000 scale topographic map of INEGI (Instituto Nacional de Estadística, Geografía e Informática; the official mapping institution of Mexico). 1:10 000 scale orthophotographs were used to compare the boundaries between mounds. The mounds are often arranged in clusters within the deposit, especially in the distal parts (Fig. 3). The clusters were partitioned into units which were then divided into groups.

3.1. Geomorphometric data

The geomorphometric variables (Table 1) were selected considering the shape, size, direction, length, geometric characteristics of the mounds and their location in the deposit. In addition, we considered the piedmont as another parameter. All variables were measured using ILWIS GIS software (ITC, International Institute for Aerospace Survey

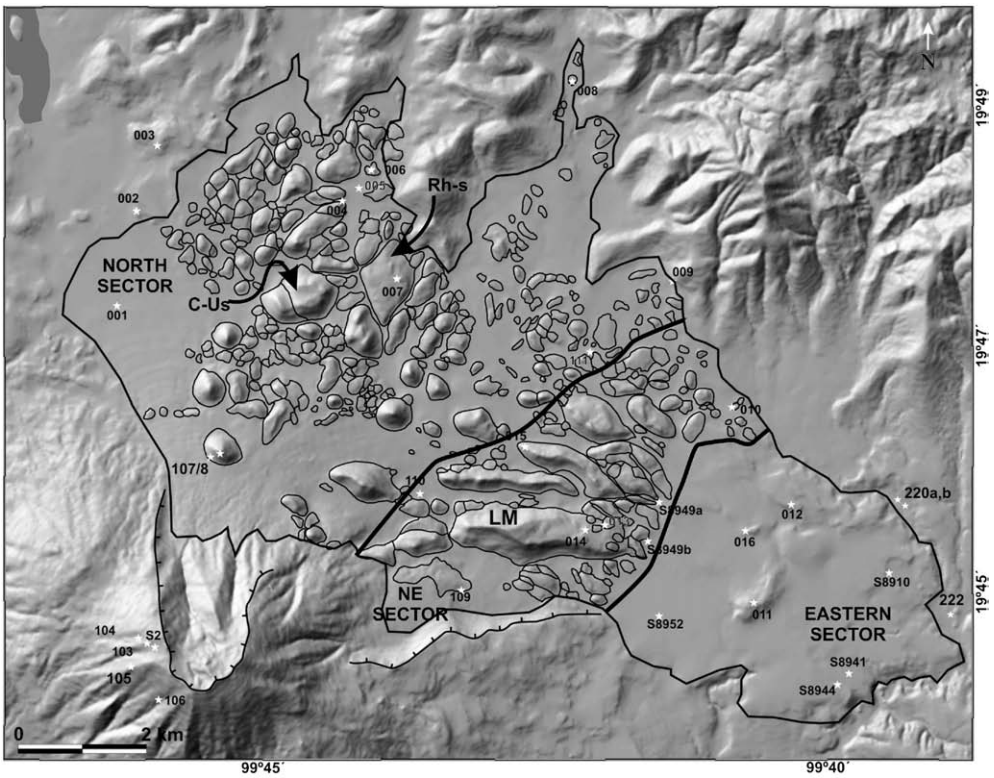

Fig. 3. Hill-shaded map of the Jocotitlán volcano showing the DAD, the morphology of hummocks and ridges and the division into three sectors: north, northeastern and eastern. The white stars are fieldwork stations (numbers starting with the letter "s" are stations used in the work of Siebe et al., 1992); C-Us: concave-upward summits; Rh-s: rhombic shapes; LM: Loma Alta Ridge.

Table 1
Geomorphometrics variables analyzed.

Geomorphometric variable	Notation and formulae		Description
Centroid	$C = \Sigma r/n^d$	(1)	Central point of the delineated units (hummocks). Is the result of adding n ratios (r) between n diameters (d).
Distance to the crater	$d = \sqrt{(x_2 - x_1)^2 + (y_2 - y_1)^2}$	(2)	Distance of the centroid to the assumed highest point of the pre-Jocotitlán edifice. (Salinas and López-Blanco, 2005).
Maximum and minimum height	H_{max}, H_{min}		Maximum and minimum height obtained by the DTM.
Media minimum height	H_{mm}		Average of the base height (Salinas and López-Blanco, 2005).
Relative height	$H_R = H_{max} - H_{min}$	(3)	Height of the hummocks with a relative topographic base.
Area	$S = \sum(a + b + c/2)$	(4)	Two dimension surface measurement (ITC, International Institute for Aerospace Survey and Earth Science, 2001).
Perimeter	P		Polygon contour distance.
Major axis	EJ_{my}		Long line that crosses the hummock or polygon water divides.
Minor axis	EJ_{mn}		Perpendicular line that cross in the middle at the major axis.
Straight axis	EJ_{rc}		Straight line that connects the ends of the major axis.
Sinuosity index	$IS = EJ_{my}/EJ_{rc}$	(5)	Ratio of the major and straight axis (Ramírez-Herrera, 1998).
Axis ratio	$D_{EJ} = EJ_{my}/EJ_{mn}$	(6)	Ratio of the major and minor axis (Salinas and López-Blanco, 2005).
Circularity index	$Cir = \pi(EJ_{rc}/2)^2/S$	(7)	Ratio of real area and the idealized circular area (Pike, 1974).
Volume	$dh = H_{max} - H_{mm}$ $V = \sum S(dh)$	(8)	Three dimensional spaces occupied for each hummock (Salinas and López-Blanco, 2005).
Slope	$P = RADDEG(Arctg\sqrt{(Dfdx^2 + Dfdy^2)})20$	(9)	Rate of change of the vertical distance in relation to the horizontal distance (ITC, International Institute for Aerospace Survey and Earth Science, 2001).
Aspect	$Dl = (ATAN2(Dx,Dy)360/2\ \pi)360$	(10)	Rate of change from the horizontal distance in relation with the lateral movement (ITC, International Institute for Aerospace Survey and Earth Science, 2001).
Piedmont	Pmt		Accumulative process area.

dh, altitudinal difference for the area (S) of each hummock or mound.
Dfdx and Dfdy are the lineal convolution filters.
ATAN2 are the inverse tangent ($\tan^{-1}$) of two input values and Arctg are the arctangents for the x and y values.
RADDEG is the trigonometric formulae to extract the slope value in degrees.

and Earth Science, 2001). The aspect value (in degree) was reclassified to ranging from 1 to 9 (north, east, south, west, northeast, southeast, southwest and northeast; flat or without direction [9] was discarded). The result was a matrix of alphabetical data which was changed to numerical data (0 to 100%) for each mound in order to standardize the values according to the number of pixels which describe each direction (Villers-Ruiz et al., 2003). To obtain the volumes of the hummocks and ridges, it was necessary to reconstruct the hypothetic pre-collapse topography (taking the reconstruction of Siebe et al., [1992; Fig. 9b] as a base model) for comparison with the actual topography.

3.2. Multivariate statistics

The final matrix was analyzed by performing a principal component analysis (PCA) which allows us to account for variance in the entire dataset, and helps us to identify the most important variables in explaining this variance. A cluster analysis was applied to the results using Euclidean distance and Pearson's "r" as measures of similarity. Nearest and farthest neighbor groups were calculated using "Statistica" software (StatSoft, Inc., 2001). Once the number of dimensions (principal components) which best describe the data was defined, the loading of important variables was optimized by varimax rotation (Dallas, 1998). The rotation involves changing the position of the eigenvectors in relation to the variables. After summarizing data variance with the PCA, the variables with the highest weight within the determined factors (Table 2) were obtained. Then, a reduction of units was performed by choosing variables with loading values that were higher than or closest to 0.9. These variables were then used to perform the cluster analysis. Finally, we made scatter plots of the main variables to identify possible correlations between them and to highlight the morphological differences existing between hummocks and ridges.

4. Results

4.1. Morphologic and stratigraphic interpretation

The spatial distribution, size, and morphology of the DAD clearly define three sectors: 1) the N sector where the majority of hummocks are located, 2) the NE sector dominated by large ridges elongated along the E–W direction, and 3) the E sector which is characterized by a quasi-flat morphology bounded by high scarps (40–80 m) (Fig. 3). It is important to note the two possible sources of the deposit: the 1.5 km wide horseshoe-shaped scarp in the main edifice; and the ca. 4.5 km long E–W scarp that cuts the eastern lower flank of the Jocotitlán volcano (Fig. 3).

4.1.1. The northern sector (N)

The N sector of the avalanche deposit is characterized by a hummocky morphology (Fig. 4A, B). Some of the hummocks are conical or elongated in shape. The deposit consists of massive andesitic to dacitic blocks and is mainly clast-supported with a sand-poor matrix suggesting a blocky lithofacies. The blocks are petrologically similar to lava flows that form the upper slope of the volcano and display distinctive cooling fractures (Fig. 4C). These blocks are sub-angular to sub-rounded in shape and range from 3 to 20 m in length. Interestingly the hummocks that are elongated are located close to clusters, and their elongation axis is oriented parallel to the flow direction.

The topographic relief is characterized by clusters of hummocks and gentle slopes between hills, without rilling or other evidence of significant erosion. When the clustered hummocks are bounded by large ridges on their rims, it is possible to observe concave summits between clusters (Fig. 3). Such summits are filled with material from the ridges on the rims and have striking rhombic shapes; sometimes, single hummocks are partially covered by these ridges (Fig. 3). This sector is also characterized by quasi-circular closed depressions which are filled by colluvium. We interpret the saddle forms that constitute the borders between some hummocks to be alluvium originating from closely-spaced mounds. After time, small piedmonts that enclose concave surfaces are formed.

4.1.2. The north eastern sector (NE)

This sector of the deposit is characterized by large ridges that lie directly north and northeast of the scarp that cuts the eastern lower flank of the Jocotitlán volcano and are parallel to this scarp (Fig. 3). It is thus deduced that they originated from the collapse of the material located between the scarp and the lower base of the volcano flank

Table 2
Loadings of the geomorphometric variables of 7 eigenvectors, resulted from the PCA, bold data indicate the variables used to perform the cluster analysis.

Variables	Download factors (Varimax rotation)						
	Extraction: principal compound						
	Tick close values to 0.90000						
	Size factor	Height factor	Geometric factor	Factor	Factor	Factor	Factor
	1	2	3	4	5	6	7
Piedmont	0.554	0.188	0.169	0.064	0.010	0.109	0.276
Perimeter	**0.964**	0.032	−0.171	0.027	0.010	0.004	−0.032
Area	**0.946**	−0.003	−0.114	0.005	0.014	−0.031	−0.105
Major Axis	**0.946**	0.028	−0.264	0.011	0.006	0.006	0.013
Minor Axis	0.888	0.126	0.245	−0.038	−0.043	0.047	0.077
Straight Axis	**0.927**	0.039	−0.237	0.016	−0.002	−0.006	−0.006
Sinuosity index	0.251	−0.074	0.435	0.019	0.129	0.068	0.243
Axis ratio	0.265	−0.037	**−0.895**	0.061	0.039	0.006	0.066
Minimum mean height	−0.019	**0.916**	0.071	−0.001	0.003	0.077	−0.042
Maximum height	0.381	0.878	0.059	0.005	0.002	0.050	−0.026
Relative height	0.830	0.395	0.014	0.006	0.015	−0.049	0.031
Volume	0.802	−0.059	−0.090	0.028	0.038	−0.064	−0.209
Main slope	0.688	0.375	0.052	0.009	−0.064	0.057	0.140
Circularity index	0.243	−0.050	**−0.933**	0.024	−0.015	−0.029	−0.000
Source distance	−0.051	−0.714	0.092	0.149	−0.213	0.149	0.048
N	0.212	0.118	0.098	0.175	0.288	0.035	−0.663
NE	0.006	0.164	0.015	−0.393	0.610	−0.284	−0.134
E	0.026	−0.096	0.077	−0.760	−0.165	−0.132	0.24
SE	0.028	−0.025	0.017	−0.106	−0.825	−0.143	0.028
S	0.090	−0.132	−0.049	0.722	−0.246	−0.236	0.076
SW	−0.019	−0.159	−0.039	0.547	0.152	0.065	0.519
W	−0.044	0.046	−0.001	−0.013	0.101	0.776	0.213
NW	−0.083	−0.110	0.056	−0.078	−0.306	0.071	−0.295
Expl. Var.	6.895	2.595	2.226	1.638	1.428	1.352	1.266
Total Prop.	0.287	0.108	0.092	0.068	0.059	0.056	0.052

(Dufresne et al., 2010). The ridges are composed of a sequence of andesitic lava flows that outcrop in a few locations. It can be inferred from the internal structure of these ridges that they initially formed a mega-block which, while sliding towards the N, shattered and fractured internally with limited dispersion and remobilization. The large (3–5 m) fractured blocks at the base of the ridges suggest an unbalanced initial mass movement compared to a translational movement (Sitar and MacLaughlin, 1997). In contrast to the debris avalanche hummocks, the elongated ridges show scattered sub-rounded blocks in their upper parts. These blocks are weathered and most possibly are products of alteration of the lavas prior to their mobilization, but rather their location is related to lateral movements between blocks (Takarada and Melendez, 2007). The characteristics of the blocks, composition (andesitic) and cooling fractures, do not match those of lava flows observed in the upper part of the main cone (Fig. 4C), which further supports the origin of these blocks as being from the faulted eastern lower volcano flank. The largest ridge, called the Loma Alta mega-block (or Toreva block) (Fig. 3), consists of partially-fragmented altered sequences of lava flows that compose the lower flank of the volcano. Contrary to what is observed in the DAD, large blocks are not present on the upper parts of other outcrop sites. However, the blocks show size homogeneity and can be fitted back into a former massive mega-block.

4.1.3. The eastern sector (E)

The eastern sector consists of a relatively flat morphology and some elongated hills with very gentle slopes. A 15–20 m high terminal scarp is found in the distal part of this unit. The deposit is distinctly more matrix-supported and better consolidated and contains sub-angular to sub-rounded clasts (Fig. 4D). Such a deposit is not observed in the middle parts of the eastern sector, but appears in the distal parts (Fig. 4E), where it has a different internal structure and emplacement mechanism compared with the N and NE sector. Concentration of Tertiary volcanic material from the southern block of the Acambay graben is evident in marginal areas of the deposit (Fig. 4F). It seems as if the avalanche behaved in this sector more as a debris flow, possibly due to the incorporation of water. The downward mass movement and the subsequent emplacement of the deposit were affected by the uneven topographic relief of the area. The pre-existing highs surrounded by the flows include an ancient dome with gentle slopes that lie in the central part of the sector (Fig.3, site 011). This dome consists of massive lava. The flanks of this dome dip at angles less than the angle of repose for angular materials (32°). The dome is covered by interbedded thick layers of black ash and white pumice possibly from the Jocotitlán. The sector is interpreted as an area filled with remobilized material from the two collapse sectors as well as pyroclastic flow deposits from the volcano. These products are covered by pumice and ash fallout deposits probably from the latest volcanic eruption of the Jocotitlán.

4.2. Statistical results

The basic statistical results show high variances, large standard deviations and a mean which does not correspond to the median. According to Freund (2004) it is necessary to have a confidence interval between 10 and 15 for a normal coefficient of variation. Hence, for this study, it is not only important to differentiate between the ridges and hummocks from the DAD but to identify whether their emplacement mechanisms were the same. Thus a high variation may be a good indicator for predicting if the units belong to different classes and also have different origins. Therefore, if ridge morphology was produced from collapse of the main edifice, they could be grouped in the same category as the other hummocks that are part of the DAD, provided that the population behaves as a normal Gaussian distribution. The elongated ridges with an E orientation could be considered a separate class of units probably not related to the same collapse, indicating two different processes for the emplacement of

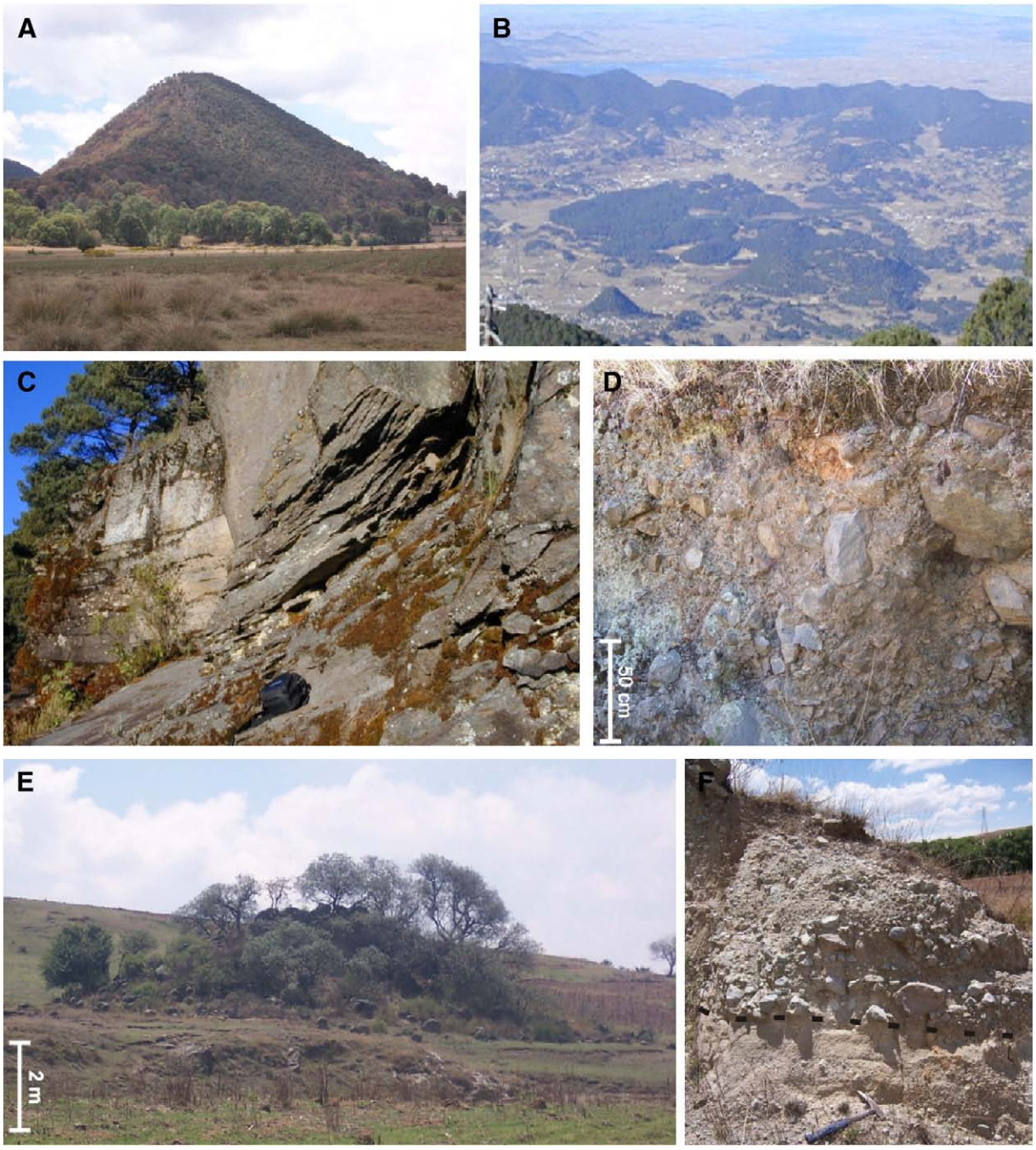

Fig. 4. Photographs of DAD (sites located in Fig. 3). A) Hummock (site 107), notice its conical shape, it is ca. 200 m high. B) View from the Jocotitlán summit, clusters of hummocks are seen in the central part of the deposit near the southern block of the Acambay graben. C) Sequence of lava flows emplaced on the southern slopes of the volcano (site 105), the lava is fractured into slabs (black bag for scale: 20 cm). D) Internal structure of the distal part of the avalanche deposit (site 220a) located near the boundary of the eastern sector. It is possible to observe sub-angular to sub-rounded clasts up to 60 cm in size, (average size of 20 cm), supported by a medium to coarse sand matrix. E) Distal hummock of the eastern sector. It does not show a continuous relation with the deposit and is smaller than hummocks of the northern sector. F) Terminal part of the avalanche deposit (site 222). This consists of heterolithological, normally graded, sub-rounded clasts in a medium to fine sandy matrix (hammer for scale). The structure, arrangement, distribution and morphology of the deposit point towards a cohesive debris flow behavior.

these deposits. In this case, the interpretations indicate processes generated by a tectonic component rather than a magmatic one.

4.3. Principal component analysis

The principal component analysis was applied to select which geomorphometric variables were important determinants. Following the selection, a Varimax rotation was carried out to maximize the variance of loadings (correlations of variables with the new compound dimensions). The results demonstrate that 7 eigenvectors incorporate 73% of the total variance. The factor loadings show that the three largest eigenvectors incorporate all 15 non-aspect variables except sinuosity (each of the remaining 4 factors account for one, two or three aspect variables) (Table 2). The first factor was named “size” because it comprises the variables longitudinally measured from the unit areas, which are the perimeter, area, major axis, straight axis; all these variables have loadings >0.9. This factor also accounts for the variables: minor axis, relative height, and mean volume with loadings >0.8. The second factor, incorporating 11.6% of the total variance, was named “height” because it contains the maximum, median, and minimum

altitudes and distance to the crater. The third factor, incorporating approximately 8% of the total variance, includes the circularity index and the axis ratio, and was thus called the "geometric" factor.

4.4. Morphometric interpretations

The multiple high loadings on each main factor indicate high correlations between variables. For that reason, variables with loadings greater than or around 0.9 were chosen for the cluster analysis. The following variables of the size factor are classified from the most to the least important, depending on the loading factor (indicated in parenthesis): perimeter (0.96), area (0.94), major axis (0.94), straight axis (0.92) (the previous variables were selected for the cluster analysis), minor axis (0.88), relative height (0.83), volume (0.80), the main slope (0.68) and piedmont (0.55). From the height factor the mean minimum altitude (0.91) was the only variable selected, but the maximum height (0.87) and the distance to the source (−0.71) have loadings above 0.7. From the geometric factor, those selected were the circularity index (0.93) and the differential index of axes (0.89). The remaining three factors are aspect variables (S, NE, SE, and W, with loading values of 0.72, 0.61, −0.82, and 0.77, respectively). The resulting dendrogram defines two groups: (i) hummocks with volumes similar to the largest elongated hummocks; and (ii) elongated geometry ridges.

The results show that the large ridges are clearly separated from the rest of the population, hence proving distinct morphological differences between the large ridges and the remaining units. The units which do not have a similarity in size with the rest of the hummocks are grouped together by solely taking into account both the circularity and axis ratio variables. However, it is noteworthy that these units have features which are common to the avalanche group, but their morphometric values are more similar to the longest elongated ridges emplaced to the E. This is an indication that at the moment of clustering, either the volume or size of the hummocks, is not as relevant as the geometric relationships between them (circularity and differential indexes of axes and the major axis). As a consequence the large elongated ridges are completely different to the avalanche hummocks.

The group with the large quantity of hummocks was divided into four sub-groups whose clustering distances are homogeneous and includes, in a general sense, the irregular and elongated hummocks which tend to be clustered. The hummocks are oriented NNE, E–W, and N; some of them have summits that are flat or slightly convex. The hummocks also have altitudinal differences of around 70 m. There is another sub-group which also comprises adjacent mounds, but it shows gentler slopes and is present in small areas within the DAD.

The N and NE sectors were used to define a clear-cut classification for each group to determine if there were certain characteristics which would allow distinguishing of the DAD ridges from the collapse group ridges. A 24-variable matrix, which expresses 46 cases, was generated by selecting units belonging to these two groups. Then, another cluster analysis was carried out using the significant variables of the first three factors. The resulting dendrogram (Fig. 5A) differentiates the larger hummocks (GMMA) from the elongated ridges of the NE sector (GMCT). The obtained results are more coherent and show preferential clustering of the possible ridges, separating the ridges of the debris avalanche associated with magmatic activity from the ridges of the debris avalanche associated with the tectonic activity of the inferred NE fault.

Using the cluster of hummocks located in the N and NE sectors (given in Fig. 3) we made scatter plots of the several morphometric variables (Fig. 5B to H). The hummocks are clearly separated at the minimum height of their base. It is observed that the ridges and their scattered hummocks occupy a lower altitudinal step compared with the hummocks in the N sector of the deposit (Fig. 5B). Normally, the height of the hummocks and ridges decreases with distance away from the source. Besides, the heights show a minor increase in the distal part, possibly due to the encountered topographic barrier (mountains of the S wall of the Acambay graben). This indicates that the deposit had sufficient momentum to climb up nearly 80 m (Fig. 5B). It is evident that the hummocks and ridges occupy the largest areas, and are concentrated in the medial part of the deposit (Fig. 5C). The ridges and the scattered hummocks of the NE sector spread a wide range of axis ratios, and the ridges have the highest values. The hummocks show maximum values of 4.5, whereas their averages are concentrated around 2. This is also evident for the circularity index, where low values are observed for the hummocks, while the ridges show a wide range (Fig. 5D); this is correlated with the sinuosity index (Fig. 5E). The hummocks have low circularity index and some of them have high sinuosity, although most ridges and scattered hummocks have low sinuosity index and high circularity index (Fig. 5E). Most data for the hummocks exhibit low values of circularity (from 0.5 to 3.0, Fig. 5F), in contrast those values for the ridges are high (>2). One of the most important variables was the perimeter; the apparent relation to the circularity shows a positive correlation for the ridges but no correlation for the scattered hummocks (Fig. 5G). Interestingly the relative height is strongly positively correlated with the slope (Fig. 5H), and the hummocks of the N sector have the highest slopes and relative heights. This is possibly related to the competence of the material (in this case represented by the silica-rich lavas that belong to the main edifice).

5. Discussion

It is possible that the E–W trending fault which cuts across the Jocotitlán volcano was activated by an earthquake related to tectonic activity within the Acambay graben. This hypothesis is supported by paleoseismic evidence of activity in the ATFS 10 000 years ago, close in time to the sector collapse event (Langridge et al., 2000). This event probably caused the fracturing and sliding of the lavas from the eastern lower flank. At the same time, the northern flank weakened and failed, triggering a debris avalanche.

Morphologically the resulting avalanche from the collapsed northern flank of the edifice shows two mechanisms of emplacement. First, the instability of the Jocotitlán edifice combined with the intrusion of a magma body in the volcano interior caused a Bezymianny-type collapse which remobilized the northern flank of the main edifice. As a result, the upper part of the remobilized northern flank slope was forced to move downwards, in part due to the momentum transmitted from the explosion, and the lower part was emplaced within the breached horseshoe-shaped crater. The debris avalanche components behaved in different ways along the runout distance. The distal part moved as a turbulent flow and, consequently, the blocks tended to superimpose onto one another, forming clusters when they encountered a topographic barrier. A second process for the formation of clusters could be the deceleration of the basal deposit (basal shear; Siebert, 1996). However, on the lateral sides of the avalanche, elongated ridges were emplaced parallel to the avalanche flow due to a lower speed of the lateral parts in comparison to the speed of the internal part of the avalanche (Fig. 6A). The hummocks tended to form more complex cluster arrangements in the center of the N sector of the DAD, to an extent that it is difficult to identify single hummocks within a cluster due to their overlapping. The central part of the avalanche gradually came to a halt allowing the materials to fill preferentially the empty spaces (Fig. 6A). A final unanswered question regarding the N sector of the DAD is why the conical hummocks occur only in this sector and are emplaced in the proximal areas of the deposit? One possible explanation could be the competence of the material (shatter-resistant) and the shorter runout distance (poor remobilization) (i.e. Thompson et al., 2010). We suggest that the smaller blocks were broken off from the larger megablocks as a result of minor flow turbulence or the natural expansion of the materials. The distal parts of the deposit show clustering of hummocks, suggesting the deceleration of the flow as a consequence of topographic barriers (Fig. 4B). Therefore, the elongated hummocks

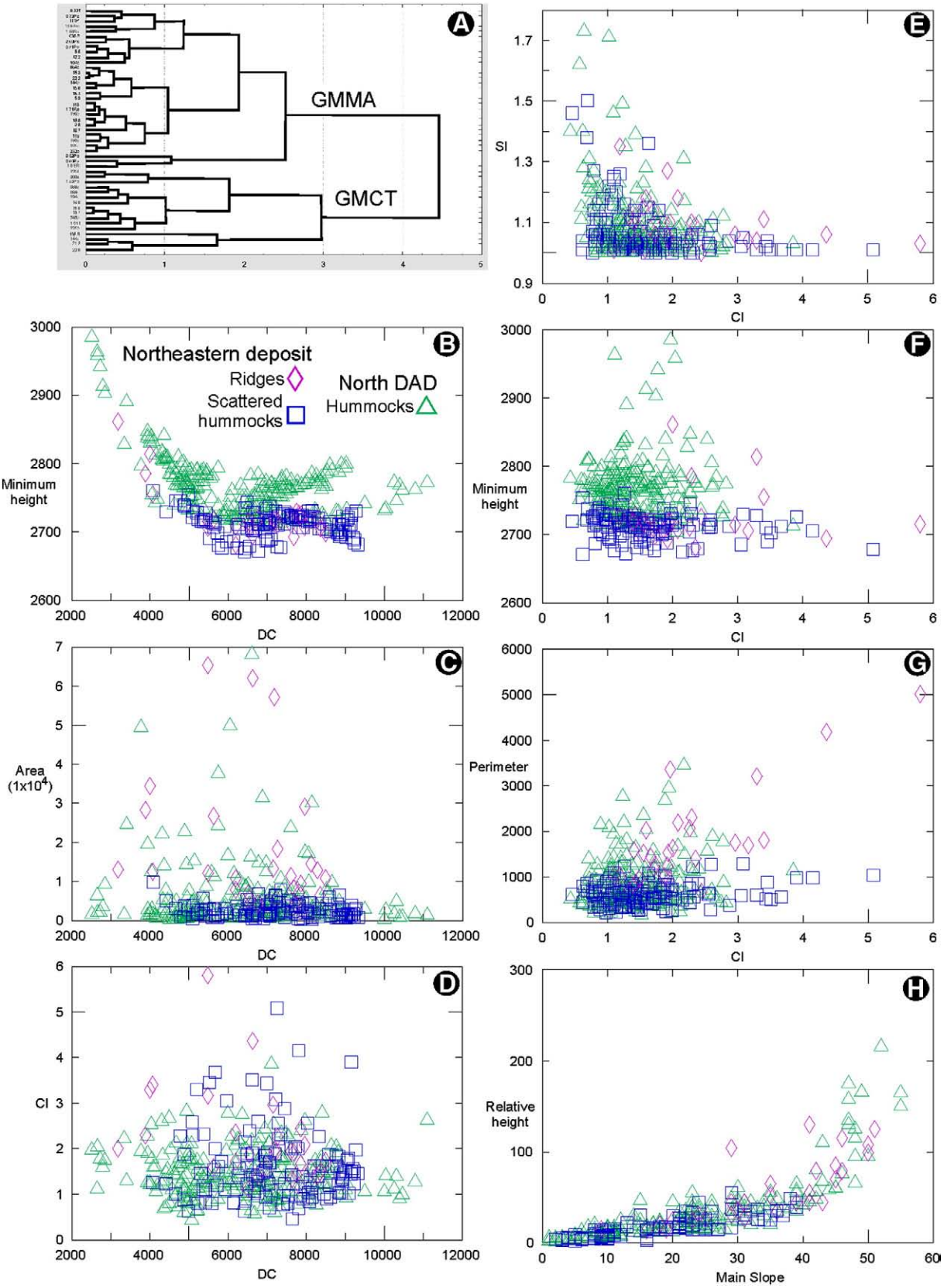

Fig. 5. A) Dendrogram showing the elongated mounds in the general cluster indicating two principal groups (see Section 4.4 in text for explanation). B), C), and D) are scatter plots of morphological characteristics of hummocks of the north (triangle) and northeastern sectors. The mounds of the northeastern sector are divided into the largest ridges (diamonds) and the minor hills or surrounding hummocks of this sector (squares). The variables are the minimum height, area (A), and circularity index (CI) vs. distance to the source or crater (DC). E), F), and G) Scatter plot of the sinuosity index, minimum height, and perimeter vs. circularity index. H) Scatter plot of the relative height vs. main slope.

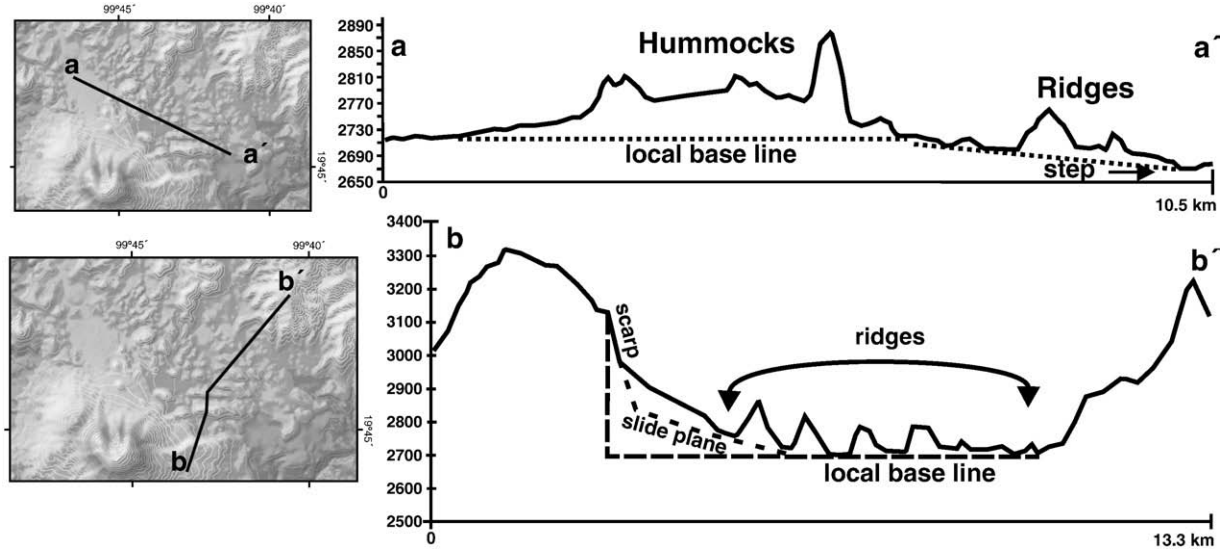

Fig. 6. A) Topographic section across the DAD. It extends laterally for 10.5 km from the lacustrine plain to the step that indicates part of the pre-avalanche topography. It is evident that the northern deposit is emplaced on a higher position with respect to the ridges emplaced 20 to 30 m below. B) Mass slide cross-section. Note that only part of the eastern flank slid down-slope. The difference in height between the scarp and the ridges is ca. 200 m.

emplaced transversally to the flow direction in this sector possibly indicate that either they encountered a topographic barrier which halted them, or they were slowed down by the agglomeration of blocks at the front of the flow.

The tectonically-triggered collapse occurred simultaneously with the gravitational failure of the main edifice to the west (N sector of DAD). Controlled by the pre-avalanche eastern fault, large mega-blocks were faulted and displaced, initiating the mobilization of large disrupted slab blocks. Some blocks were broken apart from the scarp and impacted the lacustrine plain. As a result, the lacustrine and volcaniclastic deposits were thrust-faulted and folded (Dufresne et al., 2010). The prominent blocks or ridges were emplaced obliquely to the avalanche flow due to the explosion-driven direction (Figs. 3, 6 B). This explains why the ridges have large volumes, E–W major axis directions and straight slopes. Besides, it appears that there are blocks which can be fitted back in a single mega-block (Fig. 7). In addition, the sequence of described events can be explained in terms of the reconstruction of the stress fields that caused the faulting and fracturing of the lacustrine and volcaniclastic deposits (Dufresne et al., 2010). Finally, the eastern sector was produced by the remobilization of shattered material from both sectors. This material was partially saturated with water that may have come from ancient lakes located to the north and northeastern of Jocotitlán volcano and flowed down-slope towards the eastern sector (Fig. 7). Evidence of these lakes are topographic depressions and thick lacustrine sedimentary sequences.

The geomorphometric analysis indicates that the geometric variables play an important role in distinguishing between the hummocks or ridges that originated from the volcanic avalanches and those from the tectonic collapse. Difference between the two different collapses is also reflected by the degree of fracturing of the products. Products of the N sector display a higher degree of fragmentation which probably results from its higher mobility, as well as a consequence of an elevated "collapse drop". The products of the NE sector of the deposit show lesser degrees of fragmentation, probably resulting from their origin from lower elevations in the volcano flank, and the absence of involvement of an intrusive magmatic body.

6. Conclusions

The morphological differences found throughout the DAD are keys to its origin and mode of emplacement. The analytical approach used in this study facilitated the interpretation of the patterns in the DAD morphology. The principal geomorphometric variables were the major axis, axis ratio, perimeter, circularity index, area, minimum mean height and straight axis. Specific morphological characteristics allow the identification of ridges produced by the debris avalanche; these are the difference between the major and straight axes, and the mean volumes and elongated shapes which are relatively homogeneous. With the aid of geomorphometry, it was possible to observe distinct patterns in some specific characteristics (orientation of the relief forms, changes in the size, slope and height of mounds) which allowed us to recognize differences in the deposit properties such as the type of material, degree of fracturing and the emplacement mode. Moreover, the circularity index, the axis ratio and the sinuosity index were useful parameters to classify the morphologies in this type of deposits.

Based on the obtained results, a re-interpretation of deposit morphology and emplacement was made. As a result, the entire deposit was divided into three sectors. The northern sector resulted from a main collapse of the volcano flank which was probably triggered by an earthquake and was associated with magmatic activity. The products of this collapse first behaved as a rockslide-debris avalanche before transforming to a turbulent flow at further distance from source. An inferred fault cutting across the volcano probably produced the northeast sector collapse, interpreted as tectonic collapse. The products of this collapse behaved as a translational slide. The eastern sector shows evidence of behavior as a cohesive debris flow and is partially covered by fall and pyroclastic flow deposits softening its surface morphology. The magmatic and tectonically-triggered collapses that generated the N and NE sectors of the deposit, respectively, appear to have been emplaced simultaneously during a single event.

The units that make up the hummocks which were emplaced in the proximal distances are geomorphometrically classified into two groups. There is evidence that the material which comprises each group comes from different sources. The prominent ridges are constituted by material coming from the competent massive lavas located along the eastern lower flank of the volcanic edifice, whereas the deposit of the north sector consists of remains of the former volcanic edifice of Jocotitlán. In addition, the two groups are characterized by different emplacement modes: the large ridges behaved as a collapsed mass slide, probably triggered by tectonic causes; by contrast, although the debris avalanche was initiated by the

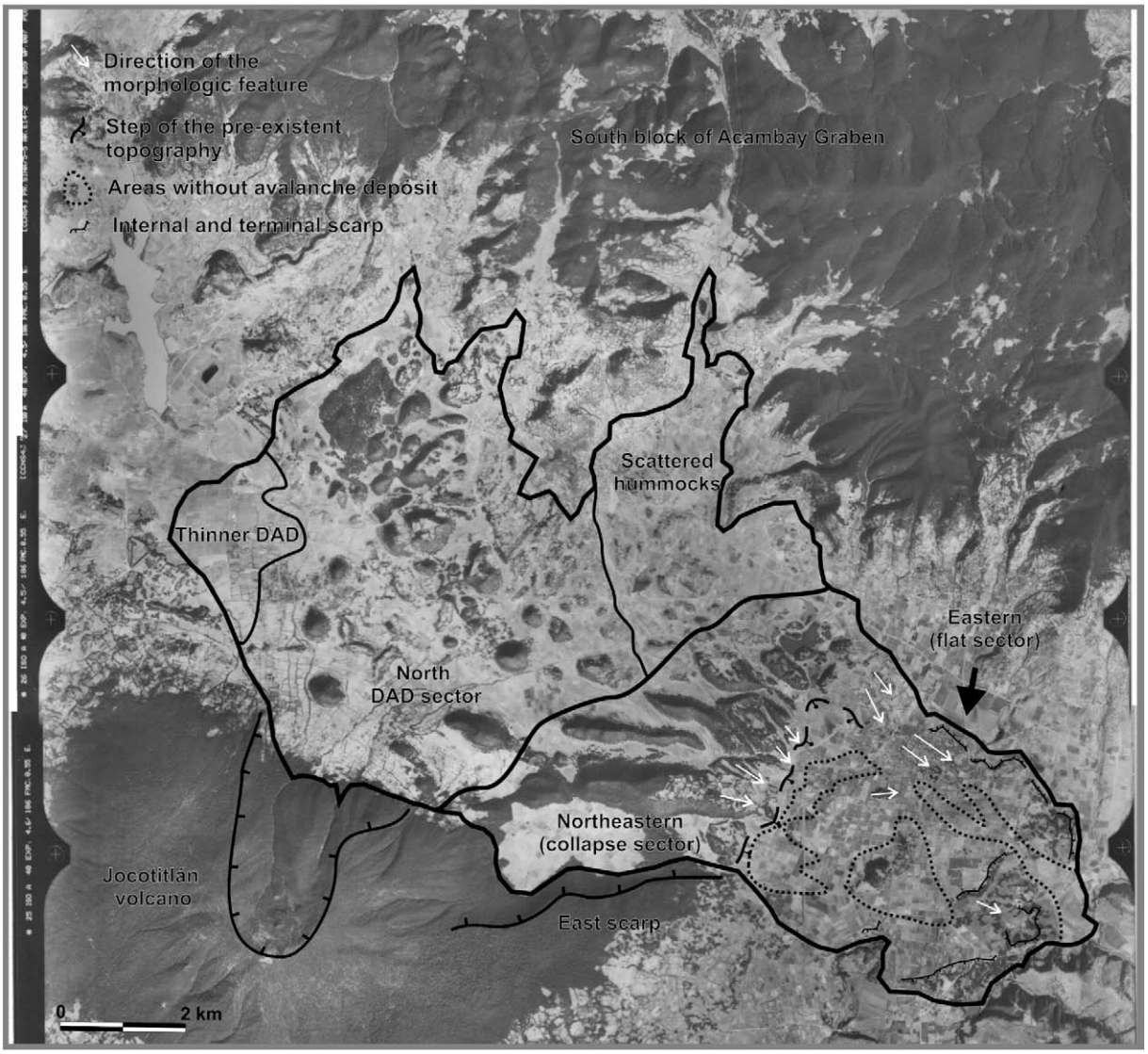

Fig. 7. Aerial photograph (1:37 500 scale), showing the distinctive of the north, northeastern and eastern sectors from of the DAD.

same mechanism, its final emplacement involved a debris flow-type mobilization. This transition in flow behavior, from rockslide-debris avalanche to a debris flow-type avalanche was probably induced by a sharp increase in the degree of fragmentation of the material. Apart from the triggering process, the potential energy and consequently the runout distance of the avalanches depositing the N and NE sectors of the deposit differed.

The analysis of morphologic characteristics, which are represented by numeric values and analyzed with multivariate analysis, allows the recognition and grading of the entire relief. The quantitative analysis of the properties of distinct surface terrain led to new geomorphological interpretations which, supported by field work and photo-interpretation, generated new evolving models of topographic relief.

Acknowledgements

We acknowledge the Instituto de Geografía, UNAM, which facilitated the development of this project. We are indebted to M. Castillo-Rodríguez and E. Muñoz-Salinas for discussion in the several fieldwork campaigns. Special thanks to J. Agustin, M.-N. Guilbaud, C. Mann, and N. Pardo, for their useful and constructive comments on review this manuscript. We would like to thank Ian S. Evans, and an anonymous reviewer for their positive and constructive suggestions for improving this paper, and Andrew Plater for his editorial handling.

References

Borgia, A., Delaney, P.T., Denlinger, R.P., 2000. Spreading volcanoes. Annual Review of Earth and Planetary Science 28, 539–570.

Capra, L., Macías, J.L., Scott, K.M., Abrams, M., Garduño-Monroy, V.H., 2002. Debris avalanche and debris flow transformed from collapse in the Trans-Mexican Volcanic Belt, Mexico — behavior, and implications for hazard assessment. Journal of Volcanology and Geothermal Research 113, 81–110.

Castillo-Rodríguez, M., López-Blanco, J., Palacios, D., 2007. Multivariate analysis of the location of rock glaciers and the environmental implications in a tropical volcano: La Malinche (Central Mexico). Zeitschrift für Geomorphologie. Supplement-bänd 51, 39–54.

Dallas, E.J., 1998. Métodos multivariados aplicados al análisis de datos. International Thomson Edts, México.

Dufresne, A., Davies, T.R., 2009. Longitudinal ridges in mass movement deposits. Geomorphology 105, 171–181. doi:10.1016/j.geomorph.2008.09.009.

Dufresne, A., Salinas, S., Siebe, C., 2010. Substrate deformation associated with the Jocotitlán edifice collapse and debris avalanche deposit. Central México. Journal of Volcanology and Geothermal Research. doi:10.1016/j.jvolgeores.2010.02.019.

Evans, I.S., 1972. General geomorphometry, derivatives of altitude, and descriptive statistics. In: Chorley, R.J. (Ed.), Spatial Analysis in Geomorphology. Harper & Row, Publishers, New York, pp. 17–90.

Evans, I.S., 1987. The morphometry of specific landforms. International Conference on Geomorphology; Part II. UK, pp. 105–124.

Ferrari, L., 2004. Slab detachment control on mafic volcanic pulse and mantle heterogeneity in central Mexico. Geology 32, 77–80.
Ferrari, L., Garduño, V.H., Pasquàre, G., Tibaldi, A., 1994. Volcanic and tectonic evolution of Central Mexico: Oligocene to present. Geofísica Internacional 33, 97–105.
Francis, P.W., Wells, G.L., 1988. Landsat Thematic Mapper observations of debris avalanche deposits in the Central Andes. Bulletin of Volcanology 50, 258–278.
Freund, J.E., 2004. Modern Elementary Statistics. Pearson, Prentice Hall, USA.
García-Palomo, A., Macías, J.L., Garduño, V.H., 2000. Miocene to recent structural evolution of the Nevado de Toluca volcano region, Central Mexico. Tectonophysics 318, 281–302.
García-Palomo, A., Zamorano, J.J., López-Miguel, C., Galván-García, A., Carlos-Valerio, V., Ortega, R., Macías, J.L., 2008. El arreglo morfoestructural de la Sierra de Las Cruces, México central. Revista Mexicana de Ciencias Geológicas 25, 158–178.
Glicken, H., 1991. Sedimentary architecture of large volcanic-debris avalanches. In: Fisher, R.V., Smith, G.A. (Eds.), Sedimentation in volcanic settings: SPEM Special Publication, 45, pp. 99–106.
ITC (International Institute for Aerospace Survey and Earth Science), 2001. Integrated Land and Water Information System (ILWIS) User´s Guide Version 3.0 Academic. International Institute for Aerospace Survey and Earth Sciences. Enschede, The Netherlands.
Langridge, R., Weldon, R., Moya, J., Suárez, G., 2000. Paleoseismology of the 1912 Acambay earthquake and the Acambay–Tixmadejé fault, Trans-Mexican Volcanic Belt. Journal of Geophysical Research 105, 3019–3037.
Lipman, P.W., Mullineaux, D.R., 1981. The 1980 eruption of Mount St. Helens, Washington. Geological Survey Professional Paper, 1250. U.S. Dept. of the Interior, U.S. Geological Survey, Washington, D.C.
Macías, J.L., 2007. Geology and eruptive history of some active volcanoes of México. In: Alaniz-Álvarez, S.A., Nieto-Samaniego, Á.F. (Eds.), Geology of México: celebrating the centenary of the Geological Society of México: Geological Society of America Special Paper, 422, pp. 183–232.
Martínez-Reyes, J., Nieto-Samaniego, A.F., 1990. Efectos geológicos de la tectónica reciente en la parte Central de México. UNAM; Revista del Instituto de Geología 9, 33–50.
Ortiz, M.A., Bocco, G.V., 1989. Análisis morfotectónico de las depresiones de Ixtlahuaca y Toluca, México. Geofísica Internacional 28, 507–530.
Palmer, A.B., Alloway, B.V., Neall, V.E., 1991. Volcanic-debris-avalanche deposits in New Zealand—lithofacies organization in unconfined, wet-avalanche flows. In: Fisher, R.V., Smith, G.A. (Eds.), Sedimentation in volcanic settings: SPEM Special Publication, 45, pp. 89–98.
Pike, R.J., 1974. Craters on earth, moon, and mars: multivariate classification and mode of origin. Earth and Planetary Science Letters 22, 245–255.
Ramírez-Herrera, M.T., 1998. Geomorphic assessment of active tectonics in the Acambay graben, Mexican Volcanic Belt. Earth Surface Processes and Landforms 23, 317–332.
Salinas, S., López-Blanco, J., 2005. Interpretation of emplacement mechanism from debris avalanche deposit by means of a geomorphometric analysis of the Jocotitlán volcano, Central México. In: Gutiérrez, F., Gutiérrez, M., Desir, G., Guerrero, J., Lucha, P., Marín, C., García-Ruiz, J.M. (Eds.), Sixth International Conference of Geomorphology, Abstracts volume, Zaragoza, Spain, p. 314.
Schaaf, P., Stimac, J., Siebe, C., Macías, J.L., 2005. Geochemical evidence for mantle origin and crustal processes in volcanic rocks from Popocatépetl and surrounding monogenetic volcanoes, Central Mexico. Journal of Petrology 46, 1243–1282.
Siebe, C., Sheridan, M.F., 1990. Reconstrucción de las diferentes fases evolutivas de crecimiento y subsecuente colapso gravitacional de los domos riolíticos localizados en las cuencas de Serdán-Oriental, Estados de Puebla y Veracruz. 2 Reunión Nacional del "Volcán de Colima". Universidad de Colima, Colima.
Siebe, C., Komorowski, J.-C., Sheridan, M.F., 1992. Morphology and emplacement of an unusual debris avalanche deposit at Jocotitlán volcano, Central Mexico. Bulletin of Volcanology 54, 573–589.
Siebe, C., Macías, J.L., Abrams, M., Rodríguez-Elizarrarás, S.R., Castro, R., Delgado, H., 1995. Quaternary explosive volcanism and pyroclastic deposits in East Central Mexico: implications for future hazards. Geological Society of America: Annual Meeting, New Orleans, LA, Field trip Guide, 1, p. 47.
Siebert, L., 1984. Large volcanic debris avalanches: characteristics of source areas, deposits and associated eruptions. Journal of Volcanology and Geothermal Research 22, 163–197.
Siebert, L., 1996. Hazards of large volcanic debris avalanches and associated eruptive phenomena. In: Scarpa, R., Tilling, R.I. (Eds.), Monitoring and mitigation of volcano hazards, pp. 541–572.
Siebert, L., Glicken, H., Ui, T., 1987. Volcanic hazards from Bezymianny- and Bandai-type eruption. Bulletin of Volcanology 49, 435–459.
Siebert, L., Béget, J.E., Glicken, H., 1995. The 1883 and late prehistoric eruptions of Augustine volcano, Alaska. Journal of Volcanology and Geothermal Research 66, 227–250.
Sitar, N., MacLaughlin, M.M., 1997. Kinematics and discontinuous deformation analysis of landslide movement. Invited Keynote Lecture. II Panamerican Symposium on Landslides, Rio de Janeiro, pp. 1–9.
StatSoft, Inc., 2001. STATISTICA (data analysis software system) version 6. www.statsoft.com.
Suter, M., Quintero, O., Johnson, C.A., 1992. Active faults and state of stress in the central part of the Trans-Mexican Volcanic Belt, Mexico 1. The Venta de Bravo Fault. Journal of Geophysical Research 97, 11,983–11,993.
Takarada, S., Melendez, C., 2007. Comparison between the emplacement mechanism of the 1991–1995 block-and-ash flows and 1792 Mayuyama debris avalanche at Unzen volcano, Japan. IUGG XXIV General Assembly Abstract, Perugia, Italy, p. 44.
Thompson, N., Bennett, M.R., Petford, N., 2010. Development of characteristic volcanic debris avalanche deposit structures: new insight from distinct element simulations. Journal of Volcanology and Geothermal Research 192, 191–200.
Villers-Ruiz, L., Trejo-Vázquez, I., López-Blanco, J., 2003. Dry vegetation in relation to the physical environment in the Baja California Peninsula, Mexico. Journal of Vegetation Science 14, 517–524.
Voight, B., Elsworth, D., 1997. Failure of volcano slopes. Geotechnique 47, 1–31.